Molecular Dynamics Simulations of Polar Polymer Brushes

Yiannis N. Kaznessis, Davide A. Hill, and Edward J. Maginn*

Department of Chemical Engineering, University of Notre Dame, Notre Dame, Indiana 46556

Received October 9, 1997; Revised Manuscript Received February 13, 1998

ABSTRACT: Brushes of end-grafted, polar polymer chains in a good, nonpolar solvent are studied via molecular dynamics simulations of a bead-spring model. The monomers are connected by finitely extensible nonlinear springs. The springs connecting consecutive monomers in a chain are labeled with dipoles parallel to the chain contour. We consider the dipoles as limits of charge pairs, replacing each dipole by a pair of charges positioned at the centers of mass of two consecutive beads. Equilibrium simulations are performed, and the static and dynamic properties of the chains are related to the dipole magnitude. It was found that the electrostatic interactions lead to a shorter brush and the collapse becomes more pronounced with increasing segmental dipole moment. The dielectric relaxation of the tethered chains is studied, and the dielectric permittivity is obtained from equilibrium dipole moment correlation functions. Results on the dielectric relaxation of tethered chains from experiments conducted by Yao et al. exhibited a broader dielectric dispersion spectrum than that of free macromolecules in homogeneous solutions. These authors attributed the results to the thermodynamic confinement (to keep uniform segment density) and the spatial confinement that prohibits a chain to cross the tethering domain boundary. The simulations indicate that neither the spatial confinement nor the thermodynamic confinement lead to a broader dielectric dispersion spectrum for the tethered chains, and we attribute the discrepancies to the morphology differences between the experimental system and the simulated one. Weak electric fields parallel and perpendicular to the grafting surface are applied, and the system response is related to the equilibrium fluctuations. We also examine the structural properties of the brushes at steady state under the influence of external electric fields.

I. Introduction

Polymer brushes are systems of macromolecules physically adsorbed or chemically end-grafted on an impermeable surface. Their technological importance stems from their wide use as colloidal stabilizers, adhesives, and lubricants. There is also much scientific interest in polymer brushes because the confinement of the one end gives rise to chain features not present in solutions of free macromolecules.

Since the first studies by Alexander[1] and DeGennes,[2] polymer brushes have been the subject of extensive research. Theoretical studies have focused on structural and thermodynamic properties employing simple scaling arguments,[1,2] self-consistent field (SCF) methods,[3−6] and computer simulations.[7−12] Experiments have investigated rheological properties of layers of tethered chains,[13−15] the kinetics of adsorption,[16,17] and the structure of brushes.[18−21] The findings of the research on polymer brushes in the last 15 years are summarized in a number of excellent reviews.[22−24]

The system we are interested in consists of polar polymer chains end-grafted on an impermeable surface and embedded in a nonpolar solvent. One of the most powerful tools for studying the conformational and dynamic properties of polar macromolecules is dielectric spectroscopy.[25,26] The conformational features can be determined by dielectric relaxation strength measurements, whereas the dielectric spectrum provides information on the dynamics of the macromolecules.

Polymers have been grouped into three categories by Stockmayer[27] depending on the monomers' dipole direction relative to the chain contour: type-A polymers, where the dipole is parallel to the chain contour, type-B, where it is perpendicular to the chain contour, and type-C, where the dipoles are located on mobile side groups. Stockmayer suggested that for type-A chains the global dipole moment of each chain is directly proportional to the chain's end-to-end vector **R**. As a result the dielectric relaxation reflects the fluctuations of **R**, establishing a connection between dielectric and low-frequency viscoelastic relaxation. Using the Rouse-Zimm normal-mode analysis,[28,29] Stockmayer indicated that only the odd-numbered modes are dielectrically active for dilute solutions of type-A flexible chains. Due to the unreversed sequence of dipoles, the first mode is the principal contributor in dielectric measurements in which an applied field drives the two chain ends in opposite directions.

The normal mode process, as the first mode relaxation was called by Adachi and Kotaka,[30] can be described formally in terms of a time correlation functions theoretical framework. Specifically the complex dielectric permittivity, defined as $\epsilon^*(\omega) = \epsilon'(\omega) - i\epsilon''(\omega)$, with ϵ' the real permittivity, ϵ'' the dielectric loss, and ω the frequency, is given by the Fourier transform of the correlation function $\phi(t)$ of the system's average dipole moment, **M**:

$$\frac{\epsilon^*(\omega) - \epsilon_\infty}{\epsilon_s - \epsilon_\infty} = \int_0^\infty \left[-\frac{\mathrm{d}\phi}{\mathrm{d}t} \right] \exp(-i\omega t)\, \mathrm{d}t \qquad (1)$$

In eq 1 ϵ_s is the static permittivity and ϵ_∞ is the permittivity limit at high frequencies. The equilibrium correlation function $\phi(t)$ of the dipole moment **M** is defined as

$$\phi(t) = \frac{\langle (\mathbf{M}(0) - \langle \mathbf{M} \rangle_0)(\mathbf{M}(t) - \langle \mathbf{M} \rangle_0) \rangle}{\langle (\mathbf{M}(0) - \langle \mathbf{M} \rangle_0)(\mathbf{M}(0) - \langle \mathbf{M} \rangle_0) \rangle} \qquad (2)$$

where $\mathbf{M} = \sum_{j=1}^n \boldsymbol{\mu}_j / n$ is the average vectorial sum of all the n dipoles in the system under study and $\langle \mathbf{M} \rangle_0$ is the equilibrium ensemble average. According to the fluc-

tuation−dissipation theorem,[31] the response of a system to a weak perturbation is entirely determined by the equilibrium correlation of the fluctuating dynamic variable that couples with the field. In other words, the normalized equilibrium correlation function of our system's dipole moment **M** is congruent to the normalized decay function $a(t)$ of the dipole moment **M**(t) when a weak field, applied at $t = -\infty$, is turned off at $t = 0$. That is

$$a(t) = 1 - b(t) = \frac{\Delta\mathbf{M}(t)}{\Delta\mathbf{M}(0)} = \phi(t) \qquad (3)$$

with $\Delta\mathbf{M}(t) = \mathbf{M}(t) - \langle\mathbf{M}\rangle_0$ being the deviation from equilibrium due to an externally imposed perturbation. $b(t)$ is the normalized build-up function describing the system's response to an externally imposed field at $t = 0$ from equilibrium to a new nonequilibrium steady state. One can consequently calculate the complex dielectric permittivity using the Fourier transform of the normalized decay function $a(t)$, instead of using eq 1.

Adachi and Kotaka[30,32,33] have determined experimentally the complex dielectric permittivity for systems of type-A macromolecules in solutions and have indicated that the relaxation for very low concentrations follows a decay determined by a series of weighted exponentials $\phi(t) = \sum_{p=1}^{\infty} w_p \exp(-t/\tau_p)$, with w_p being the weight of the pth mode of motion with a characteristic relaxation time τ_p. This is close to the normal-mode analysis prediction of the time correlation functions of type-A polymers in dilute solutions.[34] The Rouse−Zimm model provides as a consequence a useful platform for describing the dielectric relaxation of macromolecules, although as Williams has emphasized,[35] fitting the correlation function to a weighted sum of exponential decays does not necessarily mean that a distribution of relaxation times is actually present. Adachi and Kotaka also noted that deviations of their experimental results from theoretical predictions can be attributed to a number of factors, such as hydrodynamic interactions, excluded volume effects, distribution of molecular weight, and entanglement effects.

Graessley[36] performed a normal-mode analysis for tethered chains and suggested that the confinement of one end leads to twice as long a wavelength for the pth normal mode for the tethered chain as for a free chain of the same length. This in turn leads to a relaxation time four times longer for the case of tethered chains.

Yao et al.[37−39] conducted dielectric measurements on styrene (S)−isoprene (I) diblock copolymers, in the bulk, in a common solvent, and in an I-selective solvent (*n*-tetradecane). In the bulk experiments microphase separation took place and the PS blocks formed glassy domains; thus, only the motion of the polyisoprene (PI) blocks anchored on the domain boundary and confined in their own lamellae was observable. In the selective solvent system, where the S-blocks formed a rigid phase and the I-blocks were swollen, the morphology was micellar.

They found that the normal mode relaxation was retarded for all cases when compared to free homo-*cis*-polyisoprene solutions, which is consistent with Graessley's findings. However they also indicated that the relaxation spectrum, given by the dielectric loss ϵ'', is much broader for the tethered chains in the bulk and in tetradecane, even for dilute solutions, than for free

PI chains. The broader spectrum is not predicted by the Rouse−Zimm theory, as applied to tethered chains.[36] Yao et al. attributed the broadening of the spectrum to the spatial confinement that prohibits a block chain from crossing the domain boundary and the thermodynamic confinement that forces the configurations of block chains belonging to the same domain to be coupled so that the segment density profile is kept uniform. They mention though that there might be a number of other factors, which pertain to the experimental morphology, that might lead to the spectrum broadening. It is therefore interesting to investigate whether it is the confinement that leads to a broader spectrum of relaxation times or the contribution of other morphological factors of the particular experimental systems.

In this paper we present the results of MD simulations of type-A polar macromolecules grafted on an impermeable surface and embedded in a nonpolar solvent. We first examine the effect the dipoles have on the structural properties of the brush. We then study the dielectric spectrum as obtained from the equilibrium end-to-end vector correlation function, and we relate the results produced by the simulations to previous experimental results.[37−39] We have to stress here that it is not our objective to simulate the experimental systems of Yao et al. Rather we intend to use our model in idealized conditions to investigate whether the confinement of the chain end and the thermodynamic confinement (that might lead to cooperative phenomena) broaden the dielectric spectrum.

We found it interesting to investigate the linear response of polymer brushes to weak external fields, monitoring the build-up and decay of the system's polarization. The relation of the nonequilibrium response to the equilibrium fluctuations provides an important test for our simulations.

We also examine the brush structural changes at the new steady states of the system under the influence of external electric fields.

It is our intention to provide a link between simulations and dielectric spectroscopy experiments, allowing one to better comprehend the experimentally observed phenomena at the molecular level. We would also like to map the parameters of our model to real polymer quantities. Finally, it is interesting from a technological perspective to investigate methods for controlling brush properties using electric fields. One might then consider the use of brushes for the construction of electrooptical switching devices.

In the next section we describe the model and the methodology employed. In section III our simulation results are presented and discussed. Concluding remarks can be found in section IV.

II. Simulations Methodology

Molecular dynamics simulations have been utilized previously by a number of groups to examine the structure and dynamics of polymer brushes. Following in large the model used by Murat and Grest,[7] we simulated a system of M chains, each one consisting of $N + 1$ beads connected with anharmonic springs. The chains are end-grafted to an impermeable surface and embedded in a liquid solvent. The solvent is not explicitly treated; instead the monomers are coupled with a heat bath.[40,41] This approximation of solvent effects involves representing the deviation of the real force exerted by the solvent from the mean force on each

bead i by a randomly fluctuating force $\mathbf{F}_i(t)$. $\mathbf{F}_i$ is assumed to be Gaussian and delta correlated with a zero mean value

$$\langle \mathbf{F}_i(t) \rangle = 0 \tag{4}$$

The Gaussian character stems from the fact that the number of collisions of the beads with solvent molecules is large and $\mathbf{F}_i$ is formed as a sum of a very great number of random contributions. The delta correlations mean that

$$\langle F_{i\alpha}(t) F_{j\beta}(t) \rangle = 2\xi k_\mathrm{B} T m \delta_{ij} \delta_{\alpha\beta} \delta(t - t') \tag{5}$$

where α and β enumerate the Cartesian components and δ_{ij} and $\delta_{\alpha\beta}$ are Kronecker deltas. In eq 5 m is the mass of the beads and T is the temperature, which we will define shortly. ξ is the coefficient of the friction force on each bead

$$\mathbf{F}_{ri}(t) = -m\xi \frac{\mathrm{d}\mathbf{r}_i}{\mathrm{d}t} \tag{6}$$

where $\mathrm{d}\mathbf{r}_i/\mathrm{d}t$ is the velocity of the ith bead. The friction force is in fact the regular constituent of the total force exerted by the solvent. The coefficient $2m\xi T$ in eq 5 ensures the recovery of Einstein's relation $D = k_\mathrm{B} T/m\xi$ for the diffusion coefficient of the beads, when each bead is considered to perform ordinary Brownian motion.

All the beads in our system interact through the repulsive part of the Lennard−Jones potential

$$U_\mathrm{LJ}(r_{ij}) = \begin{cases} 4\epsilon\left[\left(\dfrac{\sigma}{r_{ij}}\right)^{12} - \left(\dfrac{\sigma}{r_{ij}}\right)^6 + \dfrac{1}{4}\right], & r \le r_c \\ 0, & r > r_c \end{cases} \tag{7}$$

where $r_{ij} = |\mathbf{r}_{ij}| = |\mathbf{r}_i - \mathbf{r}_j|$, σ is the bead size, ϵ is the Lennard−Jones interaction parameter, and the cutoff radius $r_c = 2^{1/6}\sigma$. This potential adequately simulates the excluded volume effect of the monomers under good solvent conditions.

Any two consecutive beads along a chain interact through a finitely extensible nonlinear elastic (FENE) potential

$$U_\mathrm{bnd}(r_{ij}) = \begin{cases} -0.5kR_0^2 \ln[1 - (r_{ij}/R_0)^2], & r \le R_0 \\ \infty, & r > R_0 \end{cases} \tag{8}$$

The FENE potential has been previously used and found to adequately describe the dynamics of bead-spring models.[40,41] In eq 8 $k = 30\epsilon/\sigma$ and $R_0 = 1.5\sigma$. This choice of parameters ensures that any two bonds do not cross each other.[7] The first bead of each chain is firmly attached on the surface at $z = 0$. A strongly repulsive potential is utilized for the interaction of the rest of the beads with the wall

$$U_\mathrm{w}(z) = \epsilon\left(\frac{\sigma}{z}\right)^9 + Az + B \tag{9}$$

where the parameters A and B are chosen so that both the potential and the force vanish at $z = \sigma/2$. We thus have $A = (2^{10}) \times 9\epsilon/\sigma$ and $B = -(2^9) \times 10\epsilon$.

We consider our chains as being type-A polar macromolecules; that is, the constitutive units possess dipole moments parallel to and sequentially aligned head-to-tail along the chain contour. If μ is the dipole moment per unit contour of the chain, we label the spring
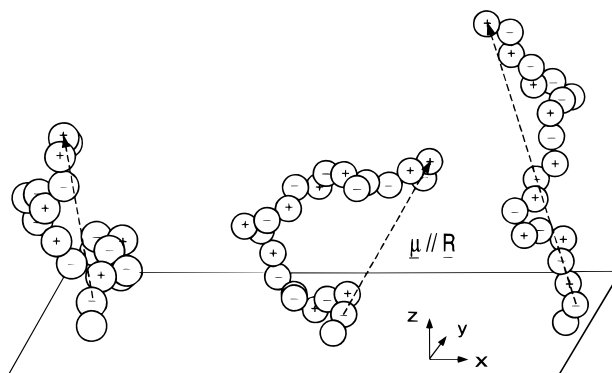

Figure 1. Schematic representation of tethered type-A polar polymers.

connecting the jth to the $(j + 1)$th beads so that the dipole vector is $\boldsymbol{\mu}_j = \mu(\mathbf{r}_{j+1} - \mathbf{r}_j)$. Since it is both conceptually and computationally easier to work with charges, we replace the dipoles μ_j by a pair of charges $q_j = -\mu/\sigma$ and $q_{j+1} = \mu/\sigma$ located at the center of mass of adjacent beads (see Figure 1). The electrostatic potential between any two beads, except any two consecutive beads constituting a dipole moment, is

$$U_\mathrm{el}(r_{ij}) = \frac{q_i q_j}{4\pi\epsilon_0 \epsilon_\mathrm{solv} r_{ij}} \tag{10}$$

where ϵ_0 is the permittivity of vacuum and ϵ_solv is the permittivity of the solvent. The first bead that is grafted on the surface is electrostatically neutral. Labeling the second bead with a negative charge, the third one with a positive charge, etc., we end up with a net polarization in the positive z direction (Figure 1). As seen in Figure 1, for type-A polar macromolecules the global chain dipole moment is parallel to the end-to-end vector. Induced dipoles are not considered in this work. The permanent dipoles do have a fluctuating magnitude, due to the fluctuations of the FENE spring length.

Application of an external electric field $\mathbf{E}$ imposes an additional force on each bead

$$\mathbf{F}_{\mathrm{E}i} = q_i \mathbf{E} \tag{11}$$

The equations of motion for the beads of our system are thus

$$m\frac{\mathrm{d}^2\mathbf{r}_i}{\mathrm{d}t^2} = -\nabla(U_\mathrm{LJ} + U_\mathrm{bnd} + U_\mathrm{w} + U_\mathrm{el}) - m\xi\frac{\mathrm{d}\mathbf{r}_i}{\mathrm{d}t} + \mathbf{F}_i + \mathbf{F}_{\mathrm{E}i} \tag{12}$$

The equations of motion were solved numerically using a fifth order predictor−corrector scheme. The time step was $\mathrm{d}t = 0.008\tau$ with $\tau = \sigma(m/\epsilon)^{1/2}$. Nondimensional units were used throughout so that $\epsilon = 1$, $\sigma = 1$, and $m = 1$. The temperature of the simulations was $k_\mathrm{B} T = 1.2\epsilon$ and the friction coefficient was $\xi = 0.5\tau^{-1}$, a value commonly used,[7] so that the inertia term does not become insignificant. The choice of the friction coefficient value in conjunction with the time step value allowed us to approximate both the random force and the systematic friction force as being constant during $\mathrm{d}t$.[42,43] The random forces are typically taken from a Gaussian distribution, but a uniform distribution with the same mean and second moment gives the same results, with significant savings in CPU time.[44] The

adequacy of this model to simulate the global motion of chains and the similarities between the model and the Rouse model have been established by the work of Grest and Kremer.[40,41]

Simulations for systems of chains with $N + 1$ beads were performed, with $N = 20$, 50, 100, at reduced surface densities $\rho_s = 0.01$, 0.03, and 0.1, with $\rho_s = M/S$, M being the number of chains used and S being the reduced surface area, $S = (L/\sigma)^2$. L is the simulation box length at the x and y coordinates. Periodic boundary conditions were used in the x and y directions, but not in the z direction. The grafting surface was considered to be at $z = 0$. A sufficiently large number of chains M was utilized, so that they did not cross the periodic boundaries more than once. Hence M ranged from 20 for the smaller chains and low grafting densities to 50 for the longer chains and higher grafting densities. The reduced dipole moment magnitudes studied were $\mu = q/\sigma$ with $q = q'/(4\pi\epsilon_0\epsilon_{solv}\sigma\epsilon)^{1/2}$ being the reduced charges (where the prime stands for nonreduced quantities). The values of the dipole moments ranged from 0.3 to 3.0. Electric fields of reduced magnitude $E/(4\pi\epsilon_0\epsilon_{solv}\sigma^3\epsilon^{-1})^{-1/2}$, ranging from 0.1 to 1.5, were applied in the x and in the z direction. The actual values of the charges and the electric fields depend on the mapping of our model to a real polymer. Such a mapping was attempted in ref 40, where one model bead was found to be equivalent to 1.73 monomers of polyisoprene, a type-A polar polymer commonly used in dielectric relaxation measurements. Given this mapping the size of the beads is $\sigma = 0.67$ nm, the mass is $m = 19.55 \times 10^{-26}$ kg, and $\tau = 10^{-10}$ s. Hence for a dipole moment $\mu' = 0.3$ D, which is of the order of the dipole that the isoprene monomers have in the direction of the chain contour,[45] the reduced charge would have a value of approximately 1.3. In the nonequilibrium simulations the fields used needed to be large enough to produce a good signal/noise ratio. It was found that for reduced charges on the order of 1.3, a reduced electric field of $E = 1.0$ would be sufficient. This is equivalent, for the system described above, to an electric field in the order of 16×10^4 V cm^{-1}. This is a very large value to be experimentally attained, but in the bead-spring model a reduced value of $E = 1.0$ produces a linear system response, as it is shown in the results section. It would be therefore easy to extrapolate to fields close to zero to obtain the polarization for experimentally utilized electric fields.

Initial configurations were generated to be close to equilibrium by growing the chains using a self-avoiding random walk scheme, with the additional limitation that the chains did not feel the surface. After the chains were grown, the system was equilibrated for times longer than the longest configurational relaxation time of the system.

A number of limitations arise due to the finite size of the sample, in view of the long range of the electrostatic interactions. Whereas the potential for dispersion interaction falls off as r^{-6}, the interaction between point charges falls only as r^{-1}. The long-range renders correlations between distant charges influential on the medium's dielectric behavior. It is thus essential to consider the interactions of distant beads in a proper fashion in the periodic boundaries framework. The correct evaluation of the electrostatic forces in molecular dynamics simulations is achieved using the Ewald summation method.[46,47] As described in Appendix A, a
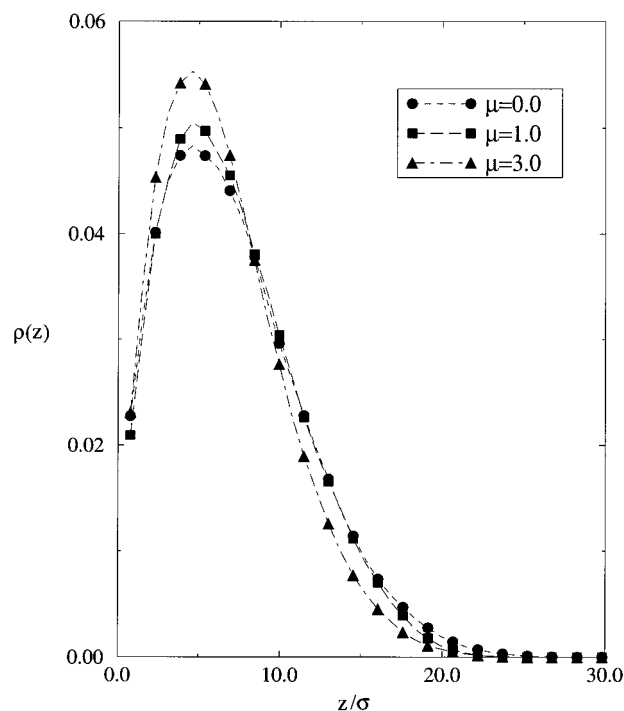

Figure 2. Monomer number density, $\rho(z)$, as a function of the distance z from the surface for systems with $N = 50$, $\rho_s = 0.01$, and different dipole moments μ.

modification of the Ewald summation scheme is needed when the system under study is infinite only in two directions.[48,49] We performed simulations using this modified Ewald summation method and found that an approximate method, where Coulomb's law is used with a cutoff range equal to half the simulation box, gives the same results with the rigorous, but more computationally demanding, Ewald method. In Appendix A we give some details of the quantitative limits of the approximate method. Consequently all the results reported herein are obtained having simulated the electrostatic interactions using the approximate method, unless otherwise indicated.

A number of computer architectures (Sun UltraSparc-140 workstations, IBM SP2, and SGI Origin 2000) were used to carry out the simulations presented here. On the Sun workstations 9×10^{-4} s of CPU time was needed per time step to simulate a system of 20 chains with $N = 20$, using the approximate method for the electrostatic potential. Using the Ewald summation for the same system required 2.6×10^{-3} s per time step, a considerably larger amount of time. To further reduce the computational time, a time decomposition parallel scheme was developed. This resulted in considerable savings in CPU times for the equilibrium runs. Efficiencies close to 90% were reached using up to eight processors. The efficiency of a parallel code is defined as $E_K = t_1/Kt_K$, where t_1 is the single node run-time and t_K the run-time of K nodes.

III. Results and Discussion

III-1. Equilibrium Properties of Type-A Polar Polymer Brushes. We begin the discussion with the structural properties of polar polymer brushes. Since the model used in this work follows in large the model used by Murat and Grest,[7] the connection can be made with equilibrium nonpolar polymer brushes studied in ref 7. An important structural quantity of polymer
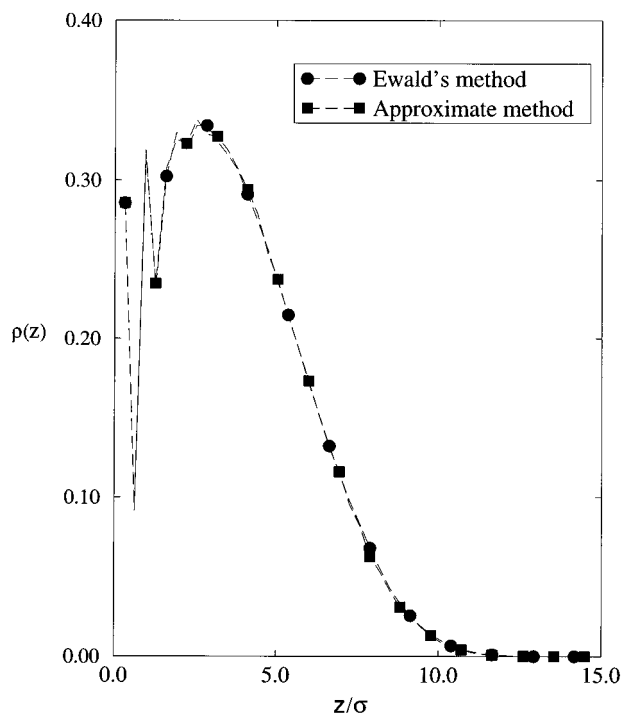
Figure 3. Monomer number density, $\rho(z)$, as a function of the distance z from the surface for a system with $N = 20$ and $\mu = 3.0$, at a surface density $\rho_s = 0.1$, using the Ewald summation and the approximate method to calculate the intermolecular electrostatic interactions.

brushes is the monomer number density $\rho(z)$. In Figure 2 we plot the monomer number density against the distance from the grafting surface for a system of $N = 50$ beads at a surface density $\rho_s = 0.01$, with different dipole moments.

As predicted by the SCF analysis and confirmed by previous computer simulations[22,23] for low and medium surface coverages, $\rho(z)$ decays following a parabolic profile. It can be observed that the parabolic profile is preserved even for highly dipolar chains, although the brush collapses slightly with increasing dipole moment. As mentioned in the previous section and described in Appendix A, a modified Ewald summation method was implemented for the calculation of the electrostatic interactions. It was found that virtually identical results could be obtained using a significantly less computationally demanding approximate method (Coulomb's law with a cutoff radius in the x and y direction equal to half the simulation box). In Figure 3 the monomer density for a system of $N = 20$ beads at a high surface density $\rho_s = 0.1$ and a large dipole moment $\mu = 3.0$ is plotted against the distance from the grafting surface. The two curves indicate results obtained by employing the approximate method and the modified Ewald summation method with an Ewald convergence factor $\eta = 0.31$ and 256 wave vectors for the reciprocal space sum. The results are identical, within the statistical error of the simulations. More details on the validity of the approximation can be found in Appendix A. Consequently in all the simulations reported here the approximate method was used. Another important structural feature is the brush average height $\langle z \rangle$, which can be calculated as the first moment of the density profile

$$\langle z \rangle = \frac{\int_0^\infty \rho(z) z \, dz}{\int_0^\infty \rho(z) \, dz} \tag{13}$$

The average brush height for a number of systems is given in Table 1. The brush height for systems with dipole moments $\mu = 1.0$ or less has almost the same value as the brush height of nonpolar systems at the same grafting density reported in ref 7. For systems with higher dipole moments the brush collapses considerably.

Other static properties are calculated and presented in Table 1, such as the height of the free ends R_z, the squared end-to-end distance

$$\langle R^2 \rangle = \langle (\mathbf{r}_1 - \mathbf{r}_N)^2 \rangle \tag{14}$$

and the squared radius of gyration

$$\langle R^2_G \rangle = \frac{1}{N} \langle \sum_{n=1}^{N} (\mathbf{r}_i - \mathbf{r}_{cm})^2 \rangle \tag{15}$$

where $\mathbf{r}_{cm}$ is the chain center of mass. Again these quantities indicate a brush collapsing with increasing dipole moment.

In a theoretical framework the brush height can be determined by free energy balances. In nonpolar brushes the balance is attained between the osmotic pressure of the monomers, which is a function of the intermolecular interactions and the monomers affinity for the solvent, and the configurational elastic energy, which is of entropic nature. When highly polar type-A macromolecules are considered, the unreversed sequence of the dipoles results in a permanent polarization that works along with the elastic energy, in favor of short, dense brushes. In Appendix B we have estimated the average brush height of the polar chains as

$$\langle z \rangle \simeq \frac{z_0}{1 + \dfrac{2\pi\mu^2 \rho_s \sqrt{\rho_s} z_0^2}{3kT}} \tag{16}$$

where z_0 is the average brush height of an equilibrium nonpolar brush. The results in Table 1 do indicate that the scaling of $\langle z \rangle$ with μ in eq 16 is correct. However, to provide a more quantitative expression from simulations will require a large number of additional simulations over a wide range of dipole magnitudes. This could be the subject of future studies.

We should also note that in principle the electrostatic energy is of no significant importance in the case of solutions of type-A chains with average or small dipole moments, when compared to the total thermal energy. Typical type-A polymers, for example, polyisoprene, have dipole moments less than $\mu = 1.0$, and we have found that for these cases the consideration of the dipole−dipole interactions in the simulations does not alter the properties of the brushes. It is also of rather limited technological value to explicitly consider the role of the dipoles in the brush structural quantities, since the collapse or stretching of the chains at equilibrium can be controlled easily by changing the temperature or the solvent. It is only when coupled with external electric fields that the inclusion of dipoles will have significant effects on the static features of the brush, as we will see in a later section.

Table 1. Static Properties for Chains with N Beads and Dipole Moments μ at a Surface Coverage ρ_s[a]

N	ρ_s	μ	T/τ	$\langle R^2 \rangle$	$\langle R_z^2 \rangle$	$\langle R_G^2 \rangle$	$\langle z \rangle$
20	0.01	1.0	4000	60.8	30.2	7.5	3.5
20	0.01	2.0	4000	56.2	27.2	7.2	3.3
20	0.01	3.0	4000	53.4	25.4	7.1	3.1
20	0.03	1.0	4000	64.6	36.0	7.7	3.7
20	0.03	2.0	4000	60.3	30.9	7.5	3.5
20	0.03	3.0	4000	53.5	26.2	7.3	3.3
20	0.10	1.0	4000	77.0	53.7	8.5	4.4
20	0.10	2.0	4000	71.1	49.3	8.1	4.2
20	0.10	3.0	4000	58.6	38.4	8.0	4.0
50	0.01	1.0	8000	204.5	116.8	23.8	6.3
50	0.01	2.0	8000	188.7	109.1	22.7	6.0
50	0.03	1.0	8000	225.1	149.3	27.2	7.5
50	0.03	2.0	8000	201.5	132.9	24.2	7.2
50	0.10	1.0	8000	390.2	331.2	40.8	10.6
50	0.10	2.0	8000	363.5	318.4	37.2	10.4
100	0.01	1.0	12000	547.8	342.8	66.4	11.6
100	0.03	1.0	12000	748.2	573.4	82.4	14.0
100	0.10	1.0	12000	1285.7	1181.2	125.8	19.2

[a] The systems were simulated for times T/τ.

Table 2. Relaxation Times for the Autocorrelation Function of the Different Static Properties for Chains with N Beads and Dipole Moments μ at a Surface Coverage ρ_s

| N	ρ_s	μ	τ_R	τ_{R_z}	τ_{R_G}
20	0.01	1.0	8.5	10.8	8.4
20	0.01	2.0	9.2	11.9	8.9
20	0.01	3.0	11.6	12.2	10.7
20	0.03	1.0	11.2	13.6	6.3
20	0.03	2.0	12.0	15.5	11.3
20	0.03	3.0	16.6	18.7	15.7
20	0.10	1.0	18.9	45.6	21.6
20	0.10	2.0	27.8	56.1	24.7
20	0.10	3.0	33.2	62.5	28.4
50	0.01	1.0	85	105	84
50	0.01	2.0	101	127	95
50	0.03	1.0	122	185	109
50	0.03	2.0	158	204	133
50	0.10	1.0	433	485	397
50	0.10	2.0	510	580	495
100	0.01	1.0	521	612	442
100	0.03	1.0	1100	1250	1050
100	0.10	1.0	2700	2950	2600

Besides the static properties, dynamic properties were studied in equilibrium, calculating the autocorrelation functions of the end-to-end distance, the radius of gyration, and the height of the free ends. The normalized autocorrelation functions were calculated as

$$\phi_X(t) = \frac{\langle X(0)X(t) \rangle - \langle X \rangle^2}{\langle X(0)X(0) \rangle - \langle X \rangle^2} \quad (17)$$

where X stands for either of the structural quantities. The relaxation times τ_X were calculated using the definition

$$\tau_X = \int_0^\infty \phi_X(t)\, \mathrm{d}t \quad (18)$$

Since the simulations were carried out for a finite time period, we considered the correlation functions to be decaying as single exponentials after t_0, with $\phi_X(t_0) = 1/e$. The calculated relaxation times are presented in Table 2. In Figure 4 the autocorrelation functions of the end-to-end distance for systems with $N = 50$, $\rho_s = 0.01$, and different dipole moments are plotted against time. The collapse of the brush with increasing chain polarity results, as anticipated, in larger relaxation times.
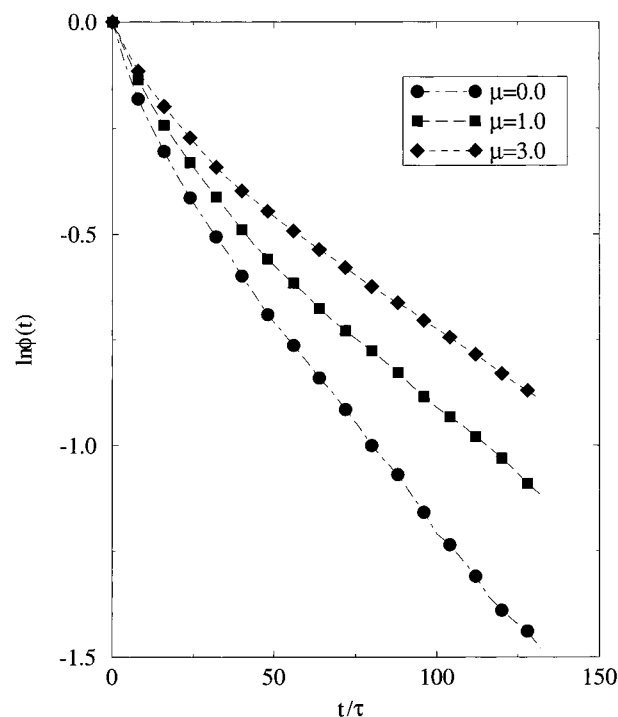
Figure 4. Autocorrelation function $\phi_R(t)$ of the end-to-end distance R for chains of $N = 50$, at a surface density $\rho_s = 0.01$ and different dipole moments.

III-2. Dielectric Relaxation of Type-A Polar Polymer Brushes. The dielectric relaxation of macromolecules end-grafted on an impermeable flat surface is the main focus of the present work. The complex dielectric permittivity ϵ^* is related to the normalized correlation function $\phi(t)$ by eq 1.

The normalized correlation function of the average dipole moment of the system is written as

$$\phi(t) = \{ \langle [\sum_{i=1}^{M} \sum_{j=1,2}^{N} \boldsymbol{\mu}_{ij}(0)][\sum_{i=1}^{M} \sum_{j=1,2}^{N} \boldsymbol{\mu}_{ij}(t)] \rangle - \langle [\sum_{i=1}^{M} \sum_{j=1,2}^{N} \boldsymbol{\mu}_{ij}] \rangle^2 \} / $$
$$\{ \langle [\sum_{i=1}^{M} \sum_{j=1,2}^{N} \boldsymbol{\mu}_{ij}(0)][\sum_{i=1}^{M} \sum_{j=1,2}^{N} \boldsymbol{\mu}_{ij}(0)] \rangle - \langle [\sum_{i=1}^{M} \sum_{j=1,2}^{N} \boldsymbol{\mu}_{ij}] \rangle^2 \} \quad (19)$$

where the sums run over all M chains and $N/2$ dipoles of each chain. Since the chains are polar type-A macromolecules, we have for the total dipole moment

$$\mathbf{M} = \sum_{i=1}^{M} \sum_{j=1}^{N} \boldsymbol{\mu}_{ij} = q \sum_{i=1}^{M} \sum_{j=1,2}^{N} (\mathbf{r}_{i(j+1)} - \mathbf{r}_{ij}) \quad (20)$$

and the correlation function of the average dipole moment is reduced to the correlation function of the end-to-end vector of the chain

$$\phi(t) = \frac{\langle \mathbf{R}_i(0) \sum_{k=1}^{M} \mathbf{R}_k(t) \rangle - \langle \mathbf{R} \rangle^2}{\langle \mathbf{R}_i(0) \sum_{k=1}^{M} \mathbf{R}_k(0) \rangle - \langle \mathbf{R} \rangle^2} \quad (21)$$

If the cross correlation terms in eq 21 are considered to be negligible, then $\phi(t)$ is reduced to the autocorrelation function given in ref 7. As observed in Figure 5 though, where we have plotted $\phi(t)$ for chains of varying number
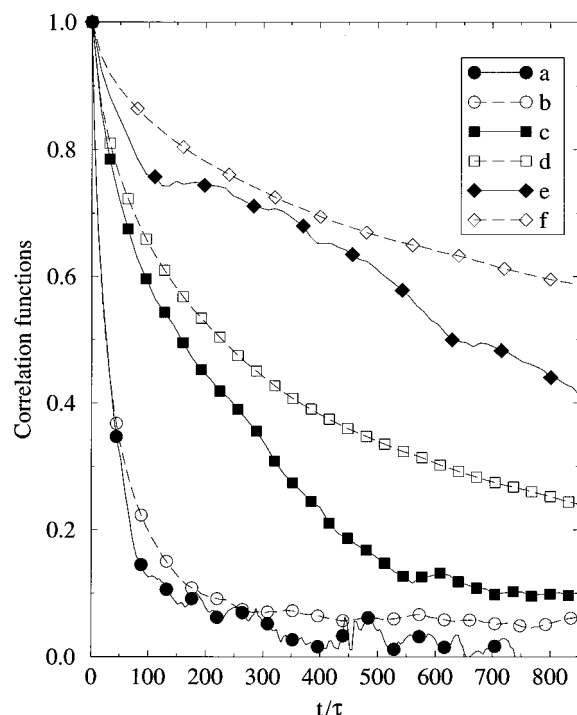
Figure 5. Total time correlation function (TCF) and autocorrelation function (ACF) of the end-to-end vector for chains of varying number of beads N with dipole moments $\mu = 1.0$ at a surface coverage $\rho_s = 0.03$. The curves show the TCF and the ACF for chains with $N = 20$ (curves a and b, respectively), $N = 50$ (curves c and d), and $N = 100$ (curves e and f).

of beads N with dipole moments $\mu = 1.0$ at a surface coverage $\rho_s = 0.03$ including and neglecting the cross correlation terms, the time correlation function of the end-to-end vector is different from the autocorrelation function of the same quantity. The difference can be explained in terms of possible cooperative phenomena in the motion of the chains, due to their preferential direction in the positive z direction. Hence the cross correlation terms should be included in the calculations of the dielectric permittivity. The faster decay of the cross correlation function can be attributed to the non-negligible cross correlation terms, which are decaying much faster than the autocorrelation terms. A parallel decay for the autocorrelation and the total correlation functions should therefore be expected for times longer than the ones needed for the cross terms to vanish. It is observed that the cross correlation function soon becomes very noisy, and one should be careful when calculating dielectric spectra from equilibrium simulations, especially for systems with longer chains.

We found it useful when taking the Fourier transform of $\phi(t)$ to first fit a function to the correlation data obtained by the simulations and then transform the function. One of the most flexible and widely used empirical functions for fitting correlation data is the Williams–Watts[50] equation

$$\phi(t) = \exp[-(t/\tau)^\beta] \qquad (22)$$

In Figure 6 the correlation functions of systems with N beads, $\mu = 1.0$, at $\rho_s = 0.03$ are plotted with the respective Williams–Watts fits. Typically the fits match $\phi(t)$ within 5% throughout the decay for systems up to $N = 50$ and $\rho_s = 0.03$. For longer chains the statistical errors in the calculation of the correlation function were in the order of 35% up to $\phi(t) = 0.6$, becoming worse for
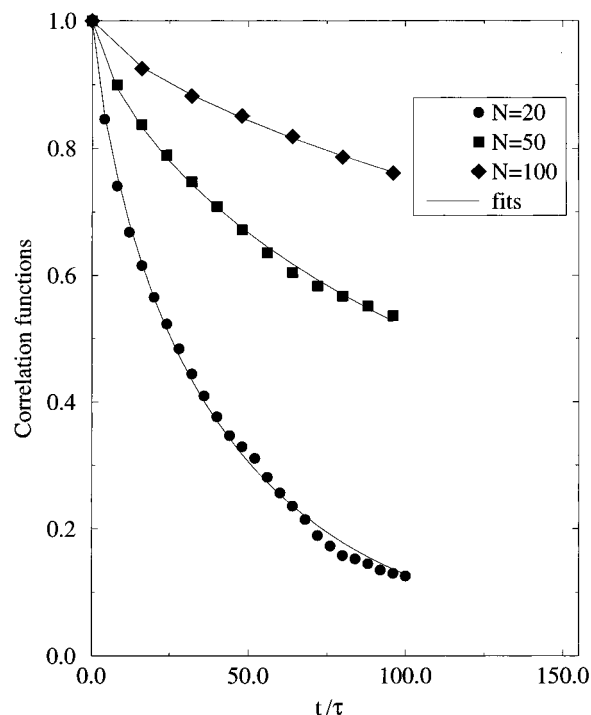

Figure 6. Time correlation functions (TCF) of the end-to-end distance vector and respective Williams–Watts fits for systems with dipole moments $\mu = 1.0$ at a surface coverage $\rho_s = 0.03$ and size of $N = 20$, $N = 50$, and $N = 100$.

Table 3. Williams–Watts Parameters τ and β from Fits to Equilibrium Time Correlation Functions of Systems with N Beads and Dipole Moments μ at Surface Coverages ρ_s

N	ρ_s	μ	τ	β
20	0.01	1.0	32.5	0.64 ± 0.02
20	0.03	1.0	40.8	0.75 ± 0.02
20	0.10	1.0	49.2	0.85 ± 0.02
50	0.01	1.0	178	0.67 ± 0.04
50	0.03	1.0	246	0.73 ± 0.04
50	0.10	1.0	271	0.71 ± 0.07

longer times. The noise in the results for the longer chains led us to consider only the first part of $\phi(t)$, which due to block averaging was the most accurate, as seen in Figure 6. The results therefore are not reliable enough for obtaining dielectric spectra of equilibrium systems with chains longer than $N = 50$, unless prohibitively large runs are performed. The way to obtain the spectra in question is to turn to nonequilibrium dynamics simulations, as will be described in a subsequent section. In Table 3 the Williams–Watts parameters τ and β calculated for the systems with chains up to $N = 50$ are presented, along with the statistical error. For the equilibrium calculations the uncertainty of the results increases with increasing chain length and grafting density, because the relaxation time becomes only a few times shorter than the whole simulation time.

The physical basis of the empirical Williams–Watts equation was examined by Ngai et al. for a number of complex systems.[51] These authors suggested that the relaxation of complex systems follows a time-dependent rate. A fundamental relaxation mode, rising from the interaction of the chains with the heat bath, dictates the decay of the correlation function at small time scales. The coupling of the chains with each other leads to a sequential cooperative adjustment of each chain to its complex environment. It provides a non-negligible
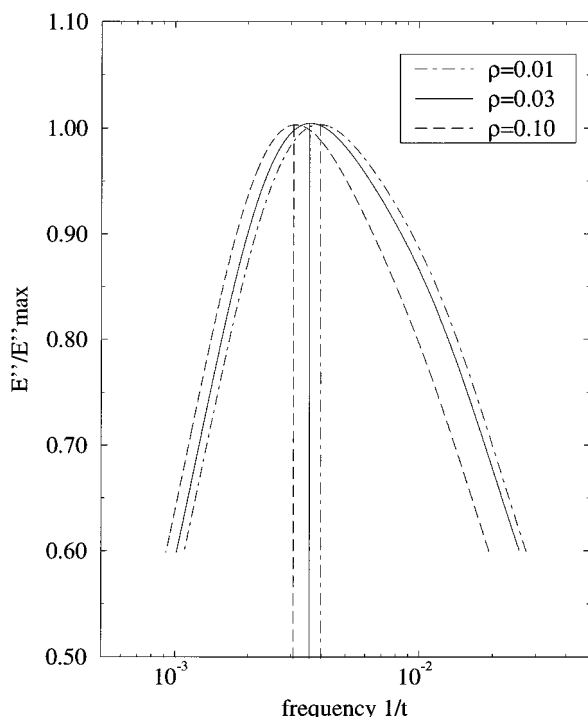
Figure 7. Reduced dielectric loss as a function of frequency for chains with $N = 50$, $\mu = 1.0$ at different surface coverages.
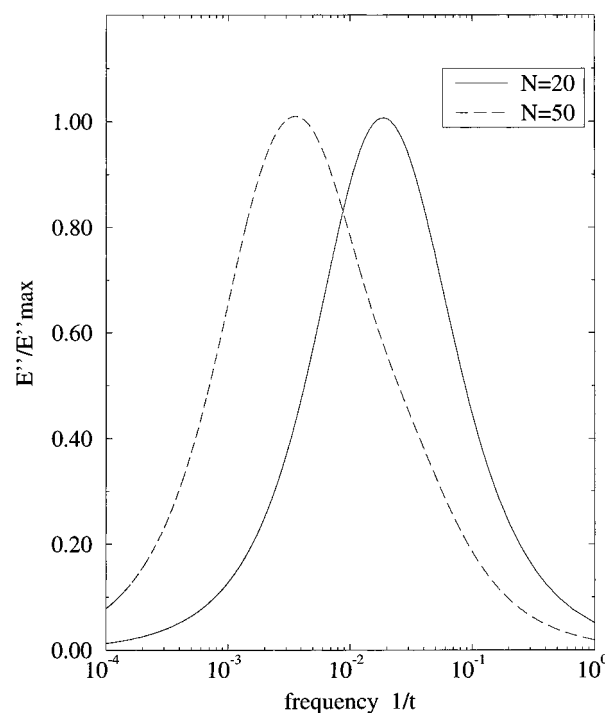
Figure 8. Reduced dielectric loss as a function of frequency for chains with $N = 20$ and $N = 50$ with dipole moments $\mu = 1.0$ at a surface coverage $\rho_s = 0.03$.

time-dependent effect slowing the simple relaxation rate at times longer than a time t_c, which is characteristic of the cooperative adjustments and is determined by the complex environment. Using such physical arguments for the rates of the relaxation Ngai et al. obtained the Williams–Watts equations, suggesting that β characterizes the coupling strength between the chains. The results support such a suggestion, although the statistical errors in the evaluation of τ and β do not allow us to make definitive statements regarding the trends. We shall return though to the calculation of τ and β with the results of the nonequilibrium simulations.

The Fourier transform of the correlation function of the end-to-end distance vector gives the real part of the dielectric permittivity and the dielectric loss. We define the reduced quantities

$$E'(\omega) = \frac{\epsilon'(\omega) - \epsilon_\infty}{\epsilon_s - \epsilon_\infty} \qquad (23)$$

and

$$E''(\omega) = \frac{\epsilon''(\omega)}{\epsilon_s - \epsilon_\infty} \qquad (24)$$

In Figure 7 we plot the reduced complex part E''/E''_{max} of the dielectric permittivity for systems of $N = 50$ beads and a dipole moment of $\mu = 1.0$ at different surface densities. As expected, the nominal relaxation time, operationally defined as $\tau_n = 1/2\pi f_{max}$, where f_{max} is the frequency that the maximum dielectric loss $E''_{max} = \epsilon''_{max}/(\epsilon_s - \epsilon_\infty)$ occurs, is larger for systems of higher surface density. In Figure 8 we observe that the maximum loss shifts to lower frequencies, that is, longer relaxation times for longer chains as anticipated.

As was described in the Introduction, Yao et al.[37−39] conducted dielectric measurements on styrene–isoprene diblock copolymers, in the bulk, in a common solvent

and in an I-selective solvent (*n*-tetradecane). In the bulk they found that for tethered type-A PI blocks the normal-mode relaxation spectrum is wider than the one of PI in homogeneous solutions, that is, not tethered on any surface. They explained this feature suggesting that the thermodynamic confinement, due to the requirement that the chains must move with minimal density fluctuations, gives rise to cooperative phenomena in the motion of the PI blocks, rendering the mode spectrum more heterogeneous than the one of free chains. They also mentioned that the spatial confinement of the PI blocks in narrow PI domains of the formed lamellar morphology could have the same effect on the relaxation spectrum. In the common solvent system the same behavior was observed for concentrations more than a critical concentration (ca. 27 wt % at 273 K), where the onset of microphase separation is expected.[38] They ascribed the broadening of the dielectric spectrum in the selective solvent system to the nonnegligible thermodynamic confinement arising from densely populated neighboring I-block chains even in the corona I-phase of an isolated micelle. They also mention that the spatial confinement that prohibits the I-block chain from crossing the hard styrene-block domain boundary could give rise to the broadening of the spectrum.

To clarify whether the factors mentioned above contribute to a broader relaxation spectrum for the tethered chains in the experiments of refs 37 and 38, we plot in Figure 9 the dielectric loss for a system of isolated tethered chains with $N = 50$ and compare it with the relaxation spectrum of a system of isolated chains in a homogeneous solution. The chains in the homogeneous solution were simulated using our model, removing the surface and applying periodic boundary conditions in the *z* direction. Initial configurations were obtained and the equilibration was performed in the same manner as for the tethered chains. The systems of the isolated chains were simulated by turning off all the intermo-
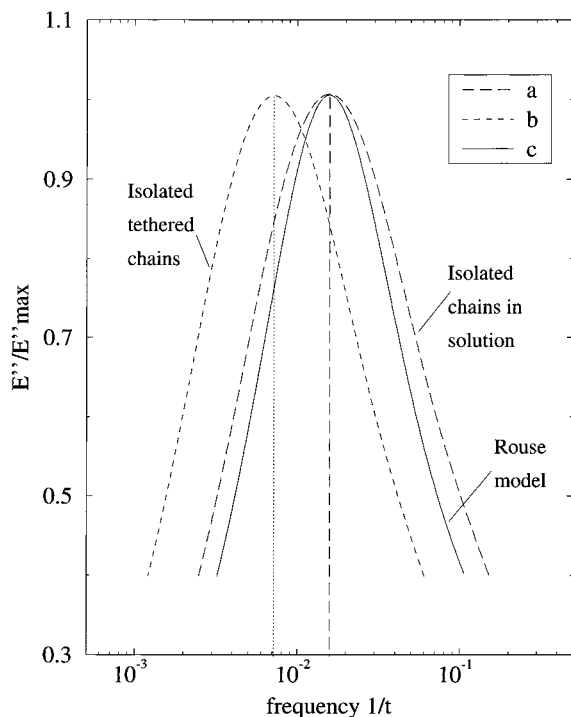
Figure 9. Reduced dielectric loss as a function of frequency for isolated chains with $N = 50$, $\mu = 1.0$ in a homogeneous solution (curve a), for isolated tethered chains with $N = 50$, $\mu = 1.0$ (curve b), and for the Rouse model (curve c).

Figure 10. Average dipole moment departure from equilibrium for chains with $N = 20$, $\mu = 2.0$ at a surface density $\rho_s = 0.1$ when external electric fields in the positive z direction with magnitudes $E_z = 0.25$, $E_z = 0.50$, $E_z = 0.75$, $E_z = 1.0$, and $E_z = 1.25$ are applied at $t = 0$.

lecular interactions. It is observed that the spectrum of the isolated tethered chains is as broad as the spectrum of the free chains in the solution. We are therefore led to conclude that it is not the confinement of the one end that broadens the spectrum. This is supported by the theoretical calculations of Graessley.[36] Also comparing the breadth of the spectrum for the isolated chains with the ones for chains at surface densities up to $\rho_s = 0.1$ in Figure 7, we are led to conclude that the thermodynamic confinement does not lead to a mode distribution broadening either.

The much broader dielectric spectra Yao et al. obtained than the ones obtained in the present work may be due to a number of other factors, such as the morphology of the experimental system, where the chains are not tethered on a flat immobile impermeable surface, the nonuniform molecular weight distribution of the experiment, entanglement effects, hydrodynamic, and excluded volume effects. Unfortunately this discrepancy of the results of the present work with the experimental ones does not allow us to attempt a mapping of the parameters of our model with real polymer properties. We anticipate though that this will be possible with simulations of macromolecules in homogeneous solutions and in melts. Is it also observed in Figure 9 that the nominal relaxation time $\tau_n = 1/2\pi f_{max}$ for the tethered chains is almost four times larger than the nominal relaxation time for the isolated chains in the homogeneous solution. This relation was predicted by Graessley[36] for the relaxation times of the autocorrelation functions of the end-to-end distance, using normal-mode analysis. In Figure 9 we have also plotted the spectrum obtained from a theoretical Rouse relaxation. The correlation of the end-to-end vector for the Rouse model is
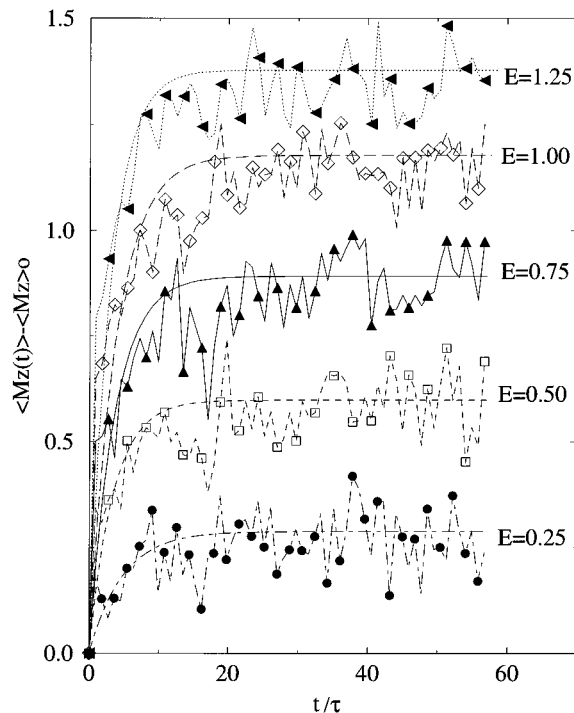
$$\phi_{Rouse}(t) = \frac{\langle \mathbf{R}(0)\mathbf{R}(t) \rangle - \langle \mathbf{R} \rangle^2}{\langle \mathbf{R}(0)\mathbf{R}(0) \rangle - \langle \mathbf{R} \rangle^2} = \frac{\displaystyle\sum_{p=1,3,5...}^{\infty} 1/p^2 \exp(-tp^2/\tau_1)}{\displaystyle\sum_{p=1,3,5...}^{\infty} 1/p^2} \quad (25)$$

with τ_1 being the relaxation time complying with the Rouse mode with $p = 1$. Although τ_1 is a function of the chain length, the friction coefficient, the bead size, and the temperature, the shape of the dielectric loss, as obtained by the Fourier transform of $\phi_{Rouse}(t)$, is the same regardless of the exact value of τ_1. In Figure 9 we plot the Rouse model complex part of the dielectric permittivity shifted in the frequency axis so that the maximum coincides with the maximum of the simulated curve for the chains in the solution. It is observed that the dielectric spectrum of both the isolated tethered chains and the isolated chains in solution is wider than the one of the Rouse model. The discrepancy of the simulated spectra from the Rouse spectrum is due to electrostatic interactions (added in proof) not considered in the Rouse model and also the inclusion of the cross correlation terms in the calculation of the simulated correlation function.

III-3. Linear Response to External Electric Fields. Application of a constant external electric field on the brush results in a net polarization in the direction of the field. The polarization, which is due to the partial alignment of the permanent dipoles in the field direction, increases with time until a long-time steady state is attained. Upon removal of the field, the polarization
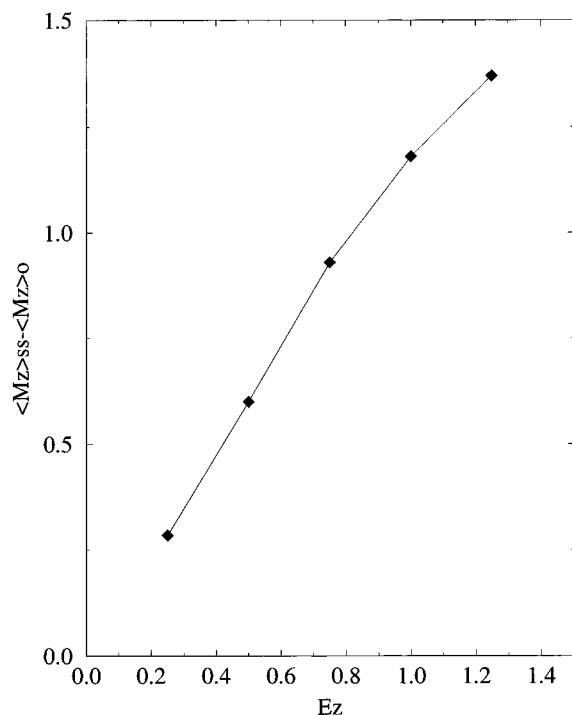
Figure 11. Average dipole moment steady-state departure from equilibrium $\langle M \rangle_{ss} - \langle M \rangle_0$ as a function of the applied electric field magnitude for a system with chains with $N = 20$, $\mu = 2.0$ at a surface density $\rho_s = 0.1$.

returns to its equilibrium value, giving rise to a dielectric relaxation. We assess the response by monitoring the system's net dipole moment, when applying a homogeneous constant electric field **E** at $t = 0$ to a system at equilibrium. Although the theory of dielectric relaxation is well documented,[52,53] local field considerations make it rather complex. For simplicity in our simulations we consider **E** as being the effective local field acting on the dipoles. In Figure 10 we plot the temporal evolution of the average system's dipole moment departure from its equilibrium value in the direction of the field $\langle M_z(t) \rangle - \langle M_z \rangle_0$, for a system of 100 chains with $N = 20$ and $\mu = 2.0$ at $\rho_s = 0.1$, when applying effective electric fields, in the positive z direction, with magnitudes $E_z = 0.25$, 0.50, 0.75, 1.0, and 1.25.

The polar chains rotate toward the direction of the field reaching a new steady state at time τ_b. The average dipole moment changes as

$$\langle M_z(t, E_z) \rangle = b'(t)E_z + \langle M_z \rangle_0 \tag{26}$$

The function $b'(t)$ is the non-normalized build-up function, determining the system's response to an external perturbation. In Figure 11 we plot the new steady-state values for $\langle M \rangle_{ss}$ minus the equilibrium value $\langle M \rangle_0$ as a function of the electric field magnitude. It is observed that for effective electric fields up to $E_z = 1.0$ the system exhibits a linear response, that is

$$\langle M_z(t, \lambda E_z) \rangle = \lambda \langle M_z(t, E_z) \rangle \tag{27}$$

In the linear regime the time evolution of the response can be described by the normalized build-up function $b(t)$, defined in eq 3, and related to $b'(t)$ by
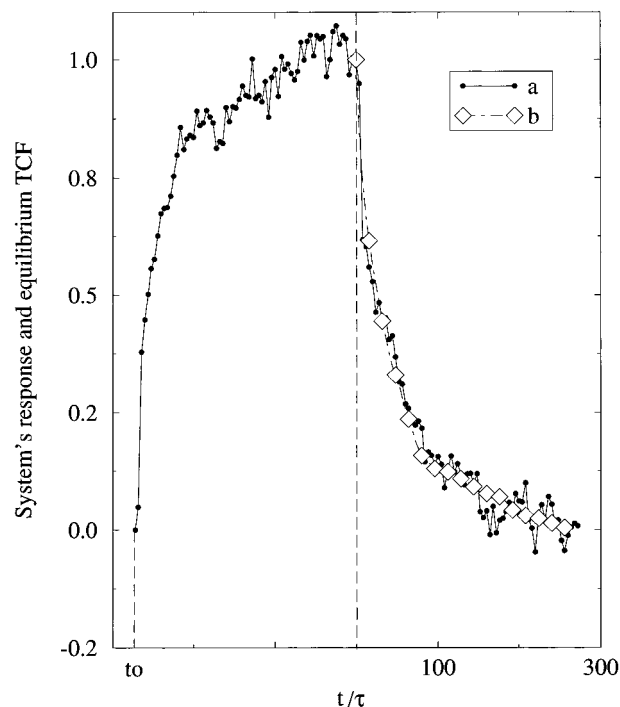

Figure 12. Average dipole moment normalized response (curve a) and equilibrium time correlation function (curve b) for chains with $N = 50$ and $\mu = 1.0$ at $\rho_s = 0.03$. An electric field $E_x = 0.8$ is applied to the system at $t = t_0$ and the build-up function is monitored until a steady state is reached. At $t = 0$ the field is turned off and the dielectric relaxation is monitored.

$$b(t) = b'(t) \frac{E}{\langle M \rangle_{ss} - \langle M \rangle_0} \tag{28}$$

In Figure 10 the build-up times are the same for fields up to $E_z = 1.0$. For $E_z > 1.0$ saturation phenomena can be observed and the system's response is no longer linear. According to Onsager's regression hypothesis, the relaxation of perturbative macroscopic departures from equilibrium is determined by the same laws as the regression of spontaneous microscopic fluctuations in an equilibrium system.[31] Onsager's hypothesis, which is a direct consequence of the fluctuation−dissipation theorem, allows us to determine the dielectric spectrum of tethered chains by monitoring the build-up or decay function of the average dipole moment when applying or turning off an external electric field, respectively. In Figure 12 we plot the response of an equilibrium system with $N = 50$ and $\mu = 1.0$ at $\rho_s = 0.03$ to a field $E_x = 0.8$ applied at time $t = t_0$ and the subsequent decay response when the field is turned off at time $t = 0$. The field results in an increase of the dipole moment in the x direction. The time evolution of this increase is determined by the normalized build-up function $b(t)$. The system reaches steady state and then we turn off the field (in the plot we do not show the steady-state fluctuations for clarity). Now the system relaxes to its equilibrium configuration following the decay function $a(t)$. As anticipated the normalized build-up function and the normalized decay function are related by $a(t) = 1 - b(t)$. In Figure 12 we also plot the correlation function $\phi(t)$ of the end-to-end vector as it was calculated from fluctuations in equilibrium. We observe that $\phi(t)$ is indeed congruent to $a(t)$, as the fluctuation dissipation theorem suggests. We should also note here that the normalized decay and build-up functions are isotropic;
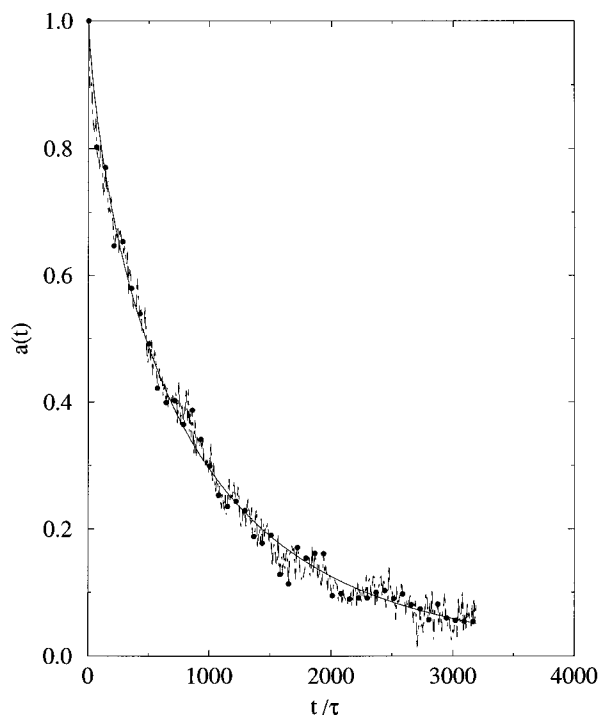
Figure 13. Normalized decay function and Williams–Watts fit of the average dipole for chains with $N = 100$, $\mu = 1.0$ at a surface coverage $\rho_s = 0.03$ under the influence of an electric field $E_x = 0.6$.

Figure 14. Reduced dielectric loss as a function of frequency for chains with $N = 100$, $\mu = 1.0$ at different surface coverages.

Table 4. Williams–Watts Parameters τ and β from Fits to Nonequilibrium Response Functions of Systems with N Beads and Dipole Moments μ at Surface Coverages ρ_s

N	ρ_s	μ	τ	β
20	0.01	1.0	26.4	0.68 ± 0.04
20	0.03	1.0	43.4	0.75 ± 0.04
20	0.10	1.0	51.9	0.83 ± 0.05
50	0.01	1.0	151	0.67 ± 0.04
50	0.03	1.0	250	0.71 ± 0.05
50	0.10	1.0	265	0.74 ± 0.07
100	0.01	1.0	670	0.72 ± 0.05
100	0.03	1.0	810	0.74 ± 0.06
100	0.10	1.0	1750	0.72 ± 0.07

that is, the response of the system to external fields parallel or perpendicular to the surface is the same, provided that the perturbation is small enough for the response to be linear.

It was mentioned in the previous section that for longer chains, equilibrium simulations do not produce accurate results for the total correlation function of the system's polarization, unless prohibitively large runs are performed. Consequently we rely on nonequilibrium simulations to obtain the dielectric spectra for chains with $N = 100$. In Figure 13 we have plotted the normalized decay function of a system with $N = 100$ and $\mu = 1.0$ at a surface coverage $\rho_s = 0.03$, when an effective electric field $E_x = 0.6$ is applied at $t = 0$. The systems were allowed to reach equilibrium before the application of the field.

One should be careful with the noise of the response signal since it can seriously affect the accuracy of the results. To minimize the noise, systems with $M = 100$ chains were used for the cases of $N = 50$ and 100, whereas systems with up to $M = 400$ chains with $N = 20$ were employed. The statistical error was independent of the size of the chains and it ranged in the order of 15% for the relaxation time τ^β. We fit the Williams–Watts equation to the normalized response signal and in Table 4 give the parameters τ and β obtained. We also provide the Williams–Watts parameters for the rest of the systems obtained from nonequilibrium simulations as a means for comparison with the equilibrium results (see Table 2). The differences between the equilibrium and the nonequilibrium results are of the order of 10% for τ^β and are due to the statistical errors in the correlation functions and the response functions. The statistical error is indicated in Table 4. For the nonequilibrium simulations it is a function of the signal/noise ratio of the response. This in turn is a function of the electric field to thermal energy ratio and
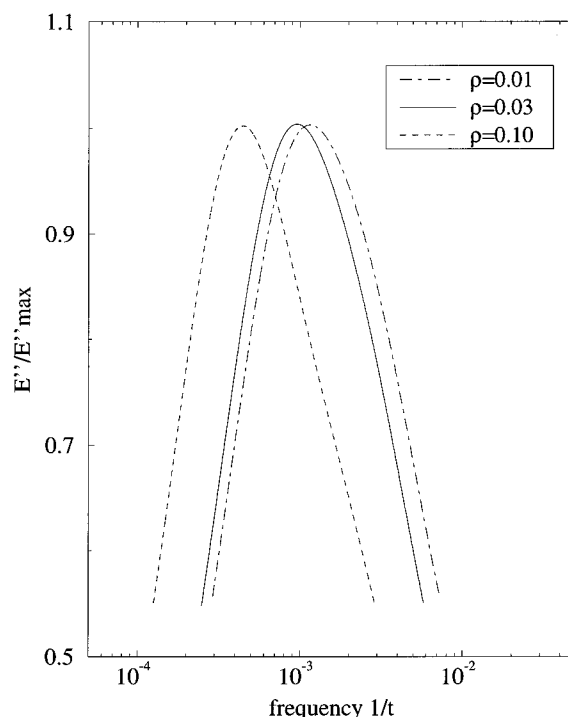
the density of the system. For dense systems fields in the linear regime produced a rather poor signal/noise ratio, compared with the signal of the less dense systems. The range of the error did not allow us to definitely conclude on the trends of β for the systems studied. This error though is not significant when evaluating the shape of the dielectric spectra and the frequency where the maximum of the loss curve occurs.

In Figure 14 we plot the dielectric spectra for the chains with $N = 100$. The results for the longer chains indicate again that the breadth of the dielectric relaxation spectrum is not affected by the spatial confinement of the one end or the thermodynamic confinement of the chains. It is also clear that nonequilibrium simulations provide an adequate means for studying the dielectric relaxation of long macromolecules.

III-4. Structural Properties of Polar Brushes under the Influence of External Electric Fields.

The electric fields perturb the conformational statistics of the brushes, and from a technological point of view it could be interesting to control the brush properties without changing the temperature or the solvent. We determine the structural changes of polar polymer brushes by studying the steady states under the application of electric fields. After the application of an external electric field, systems reach the steady state
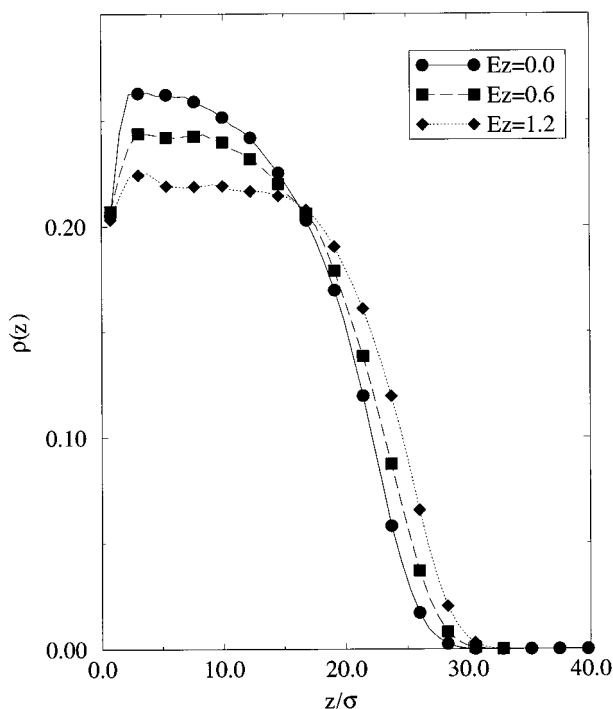
Figure 15. Monomer number density, $\rho(z)$, as a function of the distance z from the surface for systems with $N = 50$ and $\mu = 1.0$, $\rho_s = 0.10$ at equilibrium ($E_z = 0.0$) and at steady states under the influence of electric fields $E_z = 0.6$ and $E_z = 1.2$.

Table 5. Static Properties for Chains with N Beads and Dipole Moments $\mu = 1.0$ at a Surface Coverage ρ_s at Steady States under the Influence of External Electric Fields E_x or E_z

N	ρ_s	E_x	E_z	$\langle R^2 \rangle$	$\langle R_z^2 \rangle$	$\langle R_G^2 \rangle$	$\langle z \rangle$
20	0.01	0.6		64.2	27.2	8.6	3.4
20	0.01	1.2		79.2	25.7	10.0	3.3
20	0.01		0.6	72.9	53.8	8.9	4.0
20	0.01		1.2	89.3	68.3	10.1	4.5
20	0.03	0.6		66.7	28.7	8.5	3.6
20	0.03	1.2		80.8	25.5	9.9	3.4
20	0.03		0.6	76.6	61.4	9.4	4.1
20	0.03		1.2	85.8	67.9	9.9	4.5
20	0.10	0.6		81.4	39.2	9.2	4.2
20	0.10	1.2		85.2	38.5	9.5	4.0
20	0.10		0.6	78.9	67.8	10.1	4.7
20	0.10		1.2	93.7	88.7	10.9	5.1
50	0.01	0.6		244.1	108.4	26.9	6.2
50	0.01	1.2		341.9	95.0	30.4	5.9
50	0.01		0.6	246.6	187.6	24.5	7.3
50	0.01		1.2	298.2	206.4	29.8	8.1
50	0.03	0.6		303.7	138.4	32.3	7.2
50	0.03	1.2		378.5	134.4	39.9	7.0
50	0.03		0.6	275.1	205.7	27.6	8.2
50	0.03		1.2	327.4	244.1	34.2	9.0
50	0.10	0.6		416.3	321.2	42.8	10.5
50	0.10	1.2		480.2	310.2	47.1	10.3
50	0.10		0.6	466.0	409.8	43.9	11.5
50	0.10		1.2	546.5	509.5	50.5	12.3
100	0.01	0.6		737.1	355.3	81.4	11.4
100	0.03	0.6		850.5	546.4	91.6	13.8
100	0.10	0.6		1446.1	1096.6	142.7	18.9

and they are then simulated for times as long as the equilibrium runs. From the new steady-state simulations, the static properties of the nonequilibrium brush can be obtained in the same manner as they were obtained in the equilibrium calculations. In Figure 15 we plot the monomer number density for a system of chains with $N = 50$ and $\mu = 1.0$, at a surface density $\rho_s = 0.10$ at steady state under the influence of fields in the x direction and compare it with the equilibrium ($E_z = 0$) monomer number density. In Table 5 we give the static properties of the systems at steady states under the influence of electric fields in the positive z direction and in the x direction. Fields in the positive z direction result in an increase of the average brush height, whereas fields parallel to the grafting surface result in a collapsed brush. In all cases the end-to-end distance and the radius of gyration increase, whereas the height of the free ends follows the trend of the average brush height.

IV. Conclusions

In this paper we have presented molecular dynamics simulations of type-A polar polymer brushes. It was found that there is no considerable effect on the structural properties of the brushes for dipoles of low and medium magnitude. For higher dipole moments the electrostatic energy becomes of comparable magnitude with the thermal energy and the brushes collapse slightly.

A major emphasis of this paper was to contrast our simulations with experimental observations of dielectric relaxation of tethered polar polymers. Dielectric relaxation spectra were obtained from equilibrium end-to-end vector correlation functions for chains with up to $N = 50$ beads. It was found that the cross terms should be included in the calculation of the correlation function. For longer chains the equilibrium correlation function

was not accurate, since the total simulation time was only a few times larger than the relaxation times for these cases. Hence, nonequilibrium simulations were performed, applying external electric fields and monitoring the system's linear response. The dielectric spectra for chains with $N = 100$, as well as for the shorter chains, were obtained as the Fourier transform of the system's polarization response. It was found, in agreement with theoretical calculations in ref 36, that the confinement of the one end of the chains does not broaden the dielectric spectrum. It was also found that the dielectric spectrum breadth is not a function of the system's density, for the range of coverages examined. We were therefore led to conclude that it is not the thermodynamic confinement of the chains that results in a broader dielectric relaxation spectrum in the experiments of refs 37 and 38. We attributed the discrepancies of our results with the ones obtained experimentally to a number of factors such as the morphology of the experimental system, the distribution of molecular weights in the experiment, and the inadequacy of our model to account for hydrodynamic effects. These discrepancies did not allow us to attempt mapping our model's parameters to real polymer properties. We hope though that this will be possible with results from simulations of macromolecules in homogeneous solutions. We finally studied the structural properties of the brushes in the steady states under the influence of external electric fields. The ability to control the collapse and the stretching of brushes can be utilized in the construction of electrooptical switching devices. In future work we will investigate the dielectric spectra of chains in solutions and in melts.

Appendix A

In molecular dynamics simulations of dipolar systems, the long range of the electrostatic interactions greatly complicates the boundary conditions treatment. The problem was first addressed correctly by DeLeeuw and co-workers.[46] They based their method on Ewald's summation[47] for calculating electrostatic energies in large, finite pieces of ionic crystals. In this method the simulated sample under study is replicated to infinity in all three directions, resulting in a system that resembles a crystalline lattice with the simulation box as the unit cell positioned at $\mathbf{n} = (0, 0, 0)$ and the rest of the cells being characterized by the lattice vector $\mathbf{n} = (n_1, n_2, n_3)$, where n_1, n_2, and n_3 are integers. The total electrostatic energy of the unit cell is given by

$$U_{\text{els}} = \frac{1}{8\pi\epsilon_0\epsilon_{\text{solv}}} \sum_{\mathbf{n}}{}' \left(\sum_{i=1}^{N} \sum_{j=1}^{N} \frac{q_i q_j}{|\mathbf{r}_{ji}|} \right) \quad (A1)$$

where the prime on the lattice sum indicates that for $\mathbf{n} = 0$ the interactions should be omitted when $i = j$. The lattice sum in eq A1 is only conditionally convergent; that is, it does not satisfy $|U_{\text{els}}| < A|r|^{-3-\epsilon}$ for large enough $A > 0$ and $\epsilon > 0$. DeLeeuw suggested that, provided the system is charge neutral, the sum in (A1) can be written as a sum of a real space sum plus a reciprocal space sum

$$U_{\text{els}} = \frac{\sum_{i=1}^{N} \sum_{j=1}^{N} q_i q_j}{8\pi\epsilon_0\epsilon_{\text{solv}}}[\psi(\mathbf{r}_{ij}) = f(\mathbf{r}_{ij})] \quad (A2)$$

where

$$f(\mathbf{r}) = \begin{cases} \text{erfc}(\eta|\mathbf{r}|)/|\mathbf{r}|, & |\mathbf{r}| \neq 0 \\ -2\eta/\pi^{1/2}, & |\mathbf{r}| = 0 \end{cases} \quad (A3)$$

and

$$\psi(\mathbf{r}) = \sum_{\mathbf{n} \neq 0}^{\infty} (\text{erfc}(\eta|\mathbf{r} + \mathbf{n}|)/|\mathbf{r} + \mathbf{n}|) +$$
$$\frac{1}{V_{\text{cell}}} \sum_{\mathbf{m} \neq 0}^{\infty} \left(\frac{1}{\pi|\mathbf{m}|^2} \exp(-\pi^2|\mathbf{m}|^2/\eta^2) \exp(2\pi i\mathbf{m}\cdot\mathbf{r}) \right) \quad (A4)$$

where η is the Ewald convergence factor. Although the value of U_{els} does not depend on η, the computational effort of calculating the potential does depend on it. There is therefore a need for optimizing η before proceeding into a production run mode. Typically η is chosen so that the real phase terms vanish for $n > 1$ and the minimum image convention can be used. For the reciprocal space sum a sufficiently large number of wave vectors is subsequently considered to obtain the desired accuracy.

The presence of a surface requires modification of DeLeeuw's scheme, since the symmetry is no longer preserved in all three dimensions. Hautman and co-workers[48] and Perram and Ratner[49] developed a method for calculating long-range interactions in simulations where periodic boundary conditions are used in two dimensions and the sample is finite in the third one. The sample is considered to be bounded by two metallic walls in the third coordinate. The metallic walls result in the appearance of image charges positioned at mirrored cites of the original ones. Thinking of N charges q_1, q_2, ..., q_N in the simulated sample, positioned at $\mathbf{r}_1$, $\mathbf{r}_2$, ..., $\mathbf{r}_N$ with the z coordinate being bounded in both directions by metallic walls (the first one being, for example, at $z = 0$), image charges $q_{N+1...2N}$ with $q_{i+N} = -q_i$ will appear at $\mathbf{r}_{i+N} = \mathbf{r}_i - 2z_i$ for the first wall and another similar set of charges will accordingly appear for the second wall.

The cell to be reproduced in all three dimensions is now the original cell and a first image of the charges in one of the walls. Twice the number of particles have to be considered in the electrostatic interactions calculation, but the method ensures the correct application of Ewald's summation technique and the use of (A2). We applied the modified Ewald's summation method to our system of polar polymer brushes, considering the grafting surface to be metallic. Another metallic surface was positioned at $z_2 > (N + 1)\sigma$. It was found that the exact position of the second surface was of no importance, as long as there was no physical contact with the chains. We calculated the electrostatic energy and the static and the dynamic properties for a number of systems and found that in all cases for $q \leq 3.0$, even for the most concentrated systems ($\rho_s = 0.1$), the properties were the same with the ones obtained when an approximate method was used. The approximate method involves applying a cutoff radius equal to half the simulation box for the electrostatic potential in x and y directions. The estimated error for the static properties when using a cutoff distance equal to half the simulation box was for the above case of high concentration and large dipole moment less than 3%, which is of the order of the statistical error of our simulations. Using a cutoff distance equal to the Lennard−Jones potential cutoff increased the estimated error to almost 6%, whereas a cutoff radius double the Lennard−Jones potential gave results with a relative error of 3%. We chose the most conservative option and used a cutoff radius equal to half the simulation box. Of course for cases with smaller dipoles and less dense systems, a cutoff radius smaller than that could have been used without any accuracy compromise. The reason that the approximate method yields the correct result can be attributed to the small charge values, and the rather low concentrations. All of the above result in electrostatic energies much smaller than the total thermal energy of the system, rendering the use of the computationally expensive Ewald's summation technique unnecessary.

Appendix B

We now give a short derivation of eq 16 for the average brush height $\langle z \rangle$ of polar brushes. Type-A chains can be modeled by a nonpolar chain carrying the negative charge $-\mu$ at one end and the positive charge $+\mu$ at the other. The average electrostatic energy that a polymeric dipole, tethered on an impermeable surface, feels from the rest of the chains is

$$\langle U_{\text{el}} \rangle = \frac{2\pi\mu^2\rho_s}{3} \mathbf{R}\cdot\langle \mathbf{R} \rangle \int_0^{\infty} \frac{g(r)r\,\mathrm{d}r}{r^3} \quad (B1)$$

where $\langle \mathbf{R} \rangle$ is the ensemble average of the end-to-end vector, r is the distance between anchoring centers, and $g(r)$ is the radial distribution function. $g(r)$ is determined by the dipole−dipole interactions (U_{dip}) and the

excluded volume potential (U_{exc}). In a pairwise approximation framework we have

$$g(r) = \exp(-(U_{dip}(r) + U_{exc}(r))/k_B T) \qquad (B2)$$

If the dipolar interactions are weak compared to the excluded volume potentials, we can drop U_{dip} from $g(r)$ and introduce a cutoff length α for the integral in (B1), assuming that $g(r) = 0$ for $r < \alpha$ and $g(r) = 1$ for $r \geq \alpha$. We expect α to scale with the surface density as $\alpha \sim 1/\rho_s^{1/2}$. Hence, the average global dipolar energy on a flat surface is

$$\langle U_{el} \rangle = \frac{2\pi\mu^2\rho_s\sqrt{\rho_s}}{3} \mathbf{R}\cdot\langle\mathbf{R}\rangle \qquad (B3)$$

The probability of finding a chain with $\mathbf{R} \in (\mathbf{R},\mathbf{R}+d\mathbf{R})$ can be defined as $\Psi(\mathbf{R})\,dR^3$. For the polar brush we have that $\Psi = \Psi_0 \exp(-\langle U_{el}\rangle/k_B T)$, where Ψ_0 is the conformational distribution function for the nonpolar brush. The average end-to-end distance can then be written as

$$\langle\mathbf{R}\rangle = \int_0^\infty \mathbf{R}\Psi_0 \exp(-\langle U_{el}\rangle/k_B T))\,dR^3 \qquad (B4)$$

For $<U_{el}>/k_B T \ll 1$ we can write $\exp(-\langle U_{el}\rangle/k_B T) = 1 - \langle U_{el}\rangle/k_B T$. Hence

$$\langle\mathbf{R}\rangle \simeq \int_0^\infty \mathbf{R}\Psi_0\left(1 - \frac{2\pi\mu^2\rho_s\sqrt{\rho_s}}{3k_B T}\mathbf{R}\cdot\langle\mathbf{R}\rangle\right)dR^3 \quad (B5)$$

or

$$\langle\mathbf{R}\rangle \simeq \int_0^\infty \Psi_0\mathbf{R}\,dR^3 - \frac{2\pi\mu^2\rho_s\sqrt{\rho_s}}{3k_B T}\langle\mathbf{R}\rangle \cdot \int_0^\infty \Psi_0\mathbf{R}\mathbf{R}\,dR^3 \qquad (B6)$$

We have that $\int_0^\infty \Psi_0\mathbf{R}\,dR^3 = \langle\mathbf{R}\rangle_0$, the average end-to-end distance of nonpolar chains and also that $\int_0^\infty \Psi_0\mathbf{R}\mathbf{R}\,dR^3 = \langle\mathbf{R}\mathbf{R}\rangle_0$. If $\mathbf{k}$ is the unit vector in the z direction we can write $\langle\mathbf{R}\rangle\cdot\mathbf{k} = \langle z\rangle$ and $<\mathbf{R}>_0\cdot\mathbf{k} = z_0$, where z_0 is the average brush height of the equilibrium nonpolar brush. Equation B6 can now be written as

$$\langle z\rangle \simeq z_0 - \frac{2\pi\mu^2\rho_s\sqrt{\rho_s}}{3k_B T}\langle z\rangle\,\mathbf{k}\mathbf{k}:(\langle\mathbf{R}\mathbf{R}\rangle_0) \qquad (B7)$$

or

$$\langle z\rangle \simeq z_0 - \frac{2\pi\mu^2\rho_s\sqrt{\rho_s}}{3k_B T}\langle z\rangle z_0^2 \qquad (B8)$$

Rearrangement gives eq 16.

References and Notes

(1) Alexander, S. *J. Phys. (Paris)* **1977**, *38*, 983.
(2) de Gennes, P.-G. *Macromolecules* **1980**, *13*, 1069.
(3) Cosgrove, T. J.; Heath, T.; van Lent, B.; Leermakers, F.; Scheutjens, J. *Macromolecules* **1988**, *20*, 1692.
(4) Milner, S. T.; Witten, T. A.; Cates, M. E. *Macromolecules* **1988**, *21*, 2610; *EuroPhys. Lett.* **1988**, *5*, 413.
(5) Zhulina, E. B.; Borisov, O. V.; Pryamitsyn, V. A. *J. Colloid Interface Sci.* **1990**, *137*, 495.
(6) Carignano, M. A.; Szleifer, I. J. *J. Chem. Phys.* **1993**, *98*, 5006.
(7) Murat, M.; Grest, G. S. *Macromolecules* **1989**, *22*, 4054.
(8) Grest, G. S.; Murat, M. *Macromolecules* **1993**, *26*, 3108.
(9) Lai, P.-Y.; Binder, K. *J. Chem. Phys.* **1991**, *95*, 9288.

(10) Neelov, I. M.; Binder, K. *Macromol. Theory Simul.* **1995**, *4*, 119.
(11) Grest, G. S. *Phys. Rev. Lett.* **1996**, *76*, 4979.
(12) Doyle, P. S.; Shaqfeh, E. S. G.; Gast, A. P. *Phys. Rev. Lett.* **1997**, *78*, 1182.
(13) Klein, J.; Perahia, D.; Warburg, S. *Nature (London)* **1991**, *352*, 143.
(14) Klein, J.; Kumacheva, D.; Perahia, D.; Mahalu, D.; Warburg, S. *Discuss. Faraday Soc.* **1994**, *98*, 173.
(15) Klein, J.; Kamiyama, Y.; Yoshizawa, H.; Israelachvili, J. N.; Pincus, P.; Fetters, L. J. *Macromolecules* **1993**, *26*, 5552.
(16) Gast, A. P.; Munch M. R. *Polym. Commun.* **1989**, *30*, 324.
(17) Tassin, J. F.; Siemens, R. L.; Tang, W.-T.; Hadjiioannou, G.; Swalen, J. D.; Smith, B. A. *J. Phys. Chem.* **1989**, *93*, 2106.
(18) Cosgrove, T. J. *Chem. Soc., Faraday Trans.* **1990**, *86*, 1323.
(19) Auroy, P.; Auvray, L.; Leger L. *Phys. Rev. Lett.* **1991**, *66*, 719.
(20) Auroy, P.; Auvray, L.; Leger L. *Macromolecules* **1991**, *24*, 5158.
(21) Kent, M. S.; Lee, L.-T.; Farnoux, B.; Rondelez, F. *Macromolecules* **1992**, *25*, 6240.
(22) Milner, S. T. *Science* **1991**, *251*, 905.
(23) Halperin, A.; Tirrel, M.; Lodge, T. P. *Adv. Polym. Sci.* **1991**, *100*, 31.
(24) Grest, G. S.; Murat, M. In *Monte Carlo and Molecular Dynamics Simulations in Polymer Science*; Binder, K., Ed.; Oxford University Press: New York, 1995; p 476.
(25) Riande, E.; Saiz, E. *Dipole moments and Birefrigence of Polymers*; Prentice Hall: Englewood Cliffs, NJ, 1992.
(26) Adachi, K.; Kotaka, T. *Macromolecules* **1984**, *17*, 120.
(27) Stockmayer, W. H. *Pure Appl. Chem.* **1967**, *15*, 539.
(28) Rouse, P. E. *J. Chem. Phys.* **1953**, *21*, 1272.
(29) Zimm, B. H. *J. Chem Phys.* **1956**, *24*, 269.
(30) Adachi, K.; Kotaka, T. *Macromolecules* **1987**, *20*, 2018.
(31) McQuarrie, D. A. *Statistical Mechanics*; Harper and Row: New York, 1973.
(32) Adachi, K.; Kotaka, T. *Macromolecules* **1988**, *21*, 157.
(33) Adachi, K.; Kotaka, T. *J. Chem. Phys.* **1988**, *89* , 7593.
(34) Doi M.; Edwards, S. F. *The Theory of Polymer Dynamics*; Clarendon Press: Oxford, 1986.
(35) Williams, G *Chem. Rev.* **1972**, *72*, 55.
(36) Graessley, W. W. *Adv. Polym. Sci.* **1982**, *47*, 111.
(37) Yao, M.-L.; Watanabe, K.; Adachi, K.; Kotaka, T. *Macromolecules* **1991**, *24*, 2955.
(38) Yao, M.-L.; Watanabe, K.; Adachi, K.; Kotaka, T. *Macromolecules* **1991**, *24*, 6175.
(39) Yao, M.-L.; Watanabe, K.; Adachi, K.; Kotaka, T. *Macromolecules* **1992**, *25*, 1699.
(40) Kremer, K.; Grest, G. S. *J. Chem. Phys.* **1990**, *92*, 5057.
(41) Grest, G. S.; Kremer, K. *Phys. Rev. A* **1986**, *33*, 3628.
(42) van Gunsteren, W. F.; Berendsen, H. J. C.; Rullman, J. A. C. *Mol. Phys.* **1981**, *44*, 69.
(43) Allen, M. P.; Tildesley, D. J. *Computer Simulations of Liquids*; Clarendon Press: Oxford, 1987.
(44) Dünweg, B.; Paul, W. *Int. J. Mod. Phys.* **1991**, *2*, 817.
(45) Adachi, K.; Kotaka, T. *Prog. Polym. Sci.* **1993**, *18*, 585.
(46) DeLeeuw, S. W.; Perram, J. W.; Smith, E. R. *Proc. R. Soc. London* **1980**, *A373*, 27.
(47) Ewald, P. *Ann. Phys.* **1921**, *64*, 253.
(48) Hautman, J.; Halley, J. W.; Rhee, Y.-J. *J. Chem. Phys.* **1989**, *91*, 467.
(49) Perram, J. M.; Ratner, M. A. *J. Chem. Phys.* **1995**, *104*, 5174.
(50) Williams, G.; Watts, D. C. *Trans. Faraday Soc.* **1970**, *66*, 80.
(51) Ngai, K. L.; Rajagopal, A. K.; Rendell, P. W.; Teitler, S. *IEEE Trans. Elect. Insul.* **1986**, *EI21*, 313.
(52) Hill, N. E.; Vaughan, W.; Price, A. H.; Davie, M. *Dielectric Properties and Molecular Behavior*; Van Nostrand: New York, 1969.
(53) Cole, R. H. *J. Chem. Phys.* **1965**, *42*, 637.